

Supplementary Information

for

Harnessing chemoselective imine ligation for tethering bioactive molecules to platinum(IV) prodrugs

Daniel Yuan Qiang Wong, Jia Yi Lau and Wee Han Ang*

Department of Chemistry, National University of Singapore, 3 Science Drive 3, Singapore 117543.

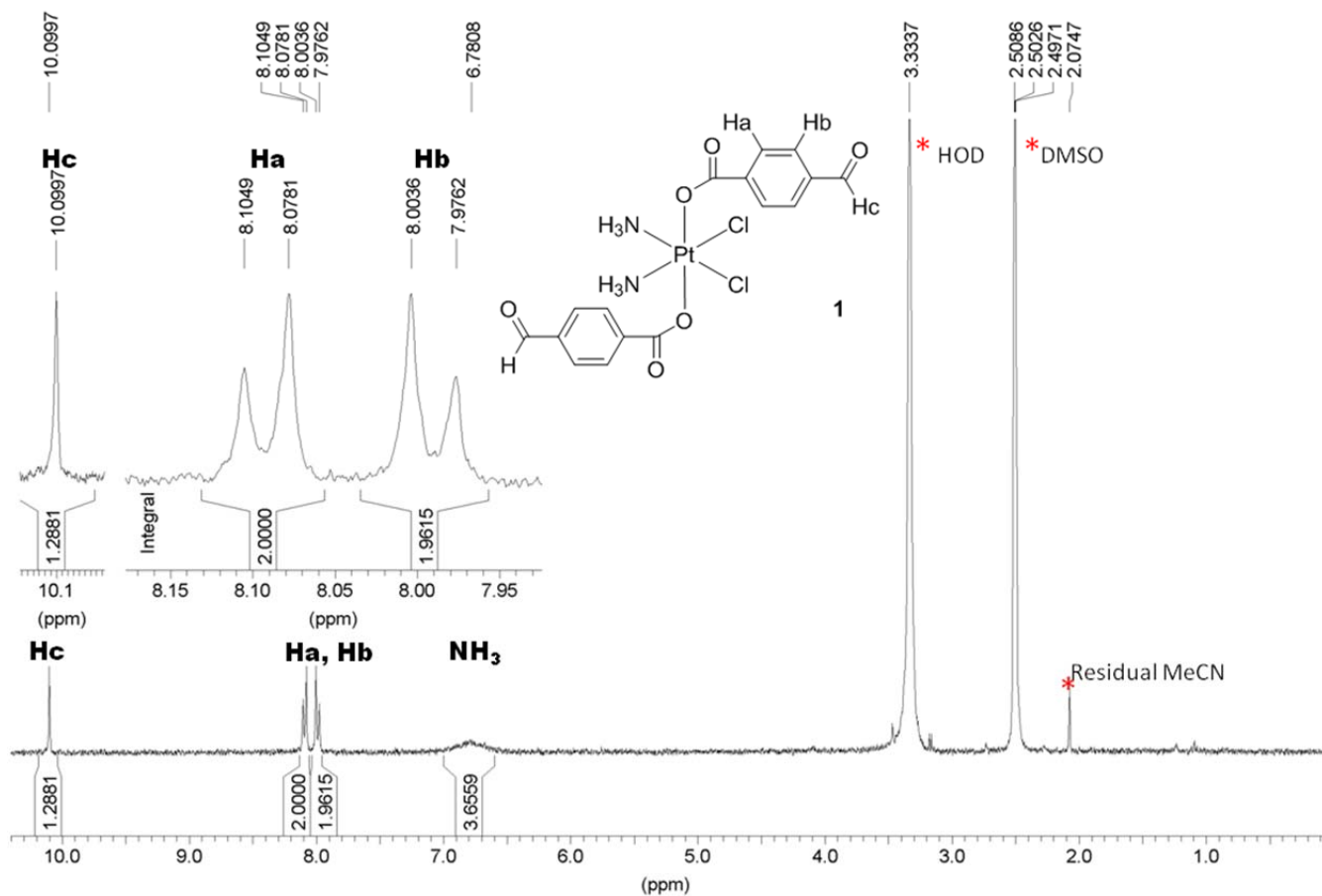


Figure S1. ¹H NMR spectra of platinum(IV)-benzaldehyde complex **1** in DMSO-d₆.

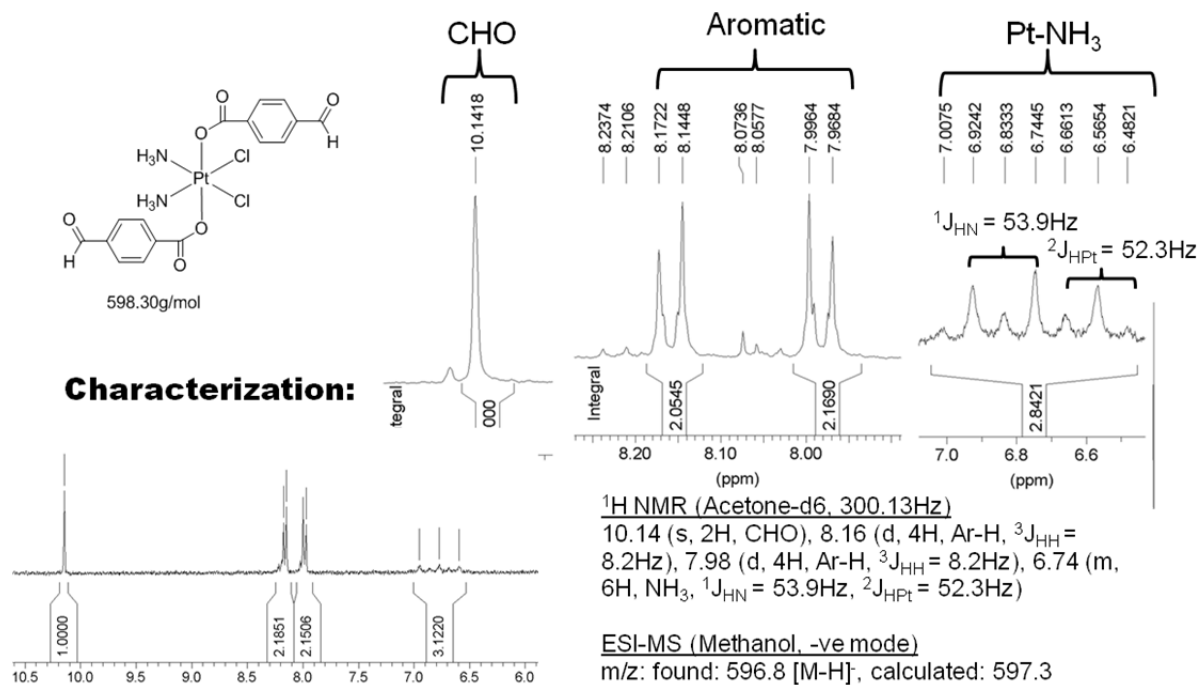
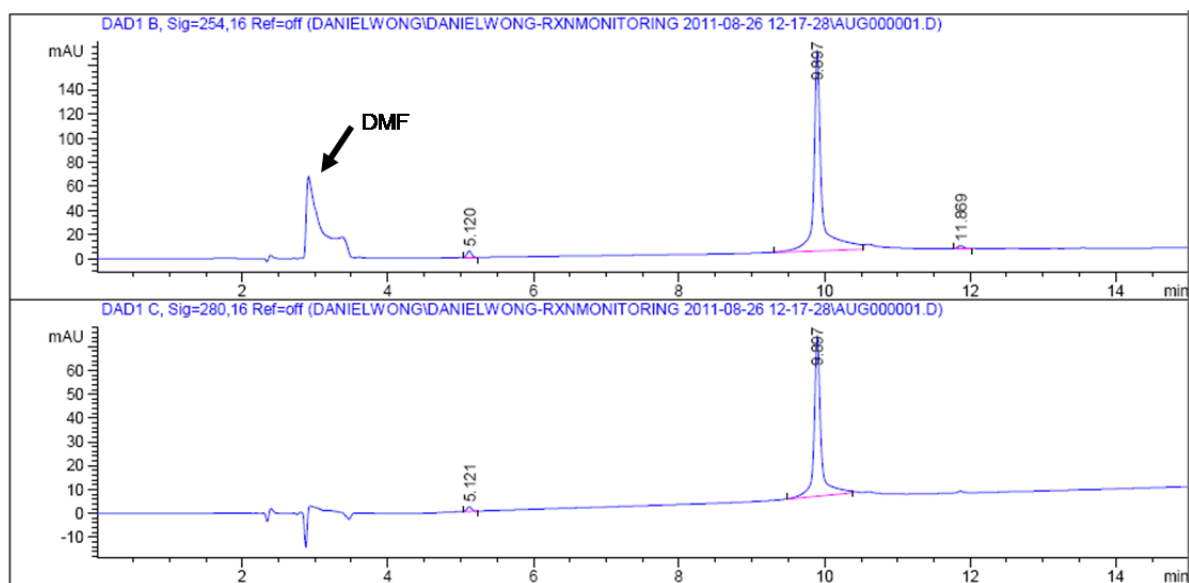


Figure S2. $^1\text{H NMR}$ spectra of complex **1** in acetone- d_6 and ESI-MS characterization.

A)



B)

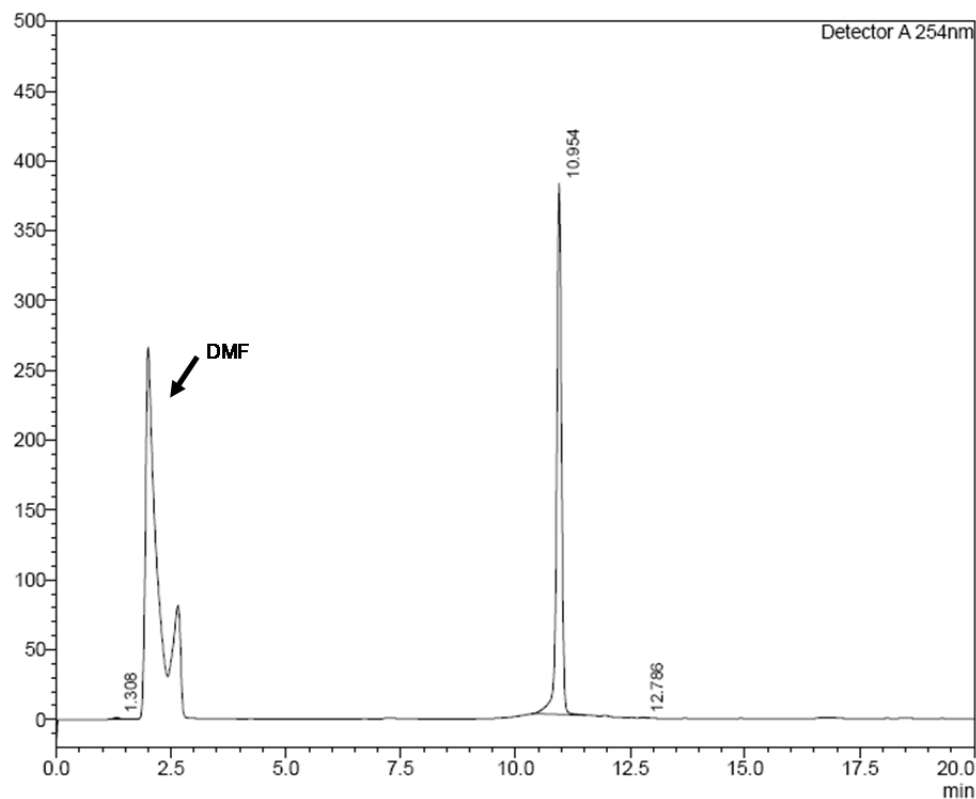


Figure S3. RP-HPLC assessment of purity of Pt-benzaldehyde **1** dissolved in DMF/ H₂O. Elution conditions for both spectra (A) and (B): 20 - 80% gradient elution system with aq. NH₄OAc buffer (10 mM, pH 5.5) (solvent A) and MeCN (solvent B) over 15 min at 1.0 mL/min. Columns used are: A) Phenomenex Luna C18(2) (250 x 4.60 mm i.d) B) Shimpack VP-ODS column (150 x 4.60 mm i.d).

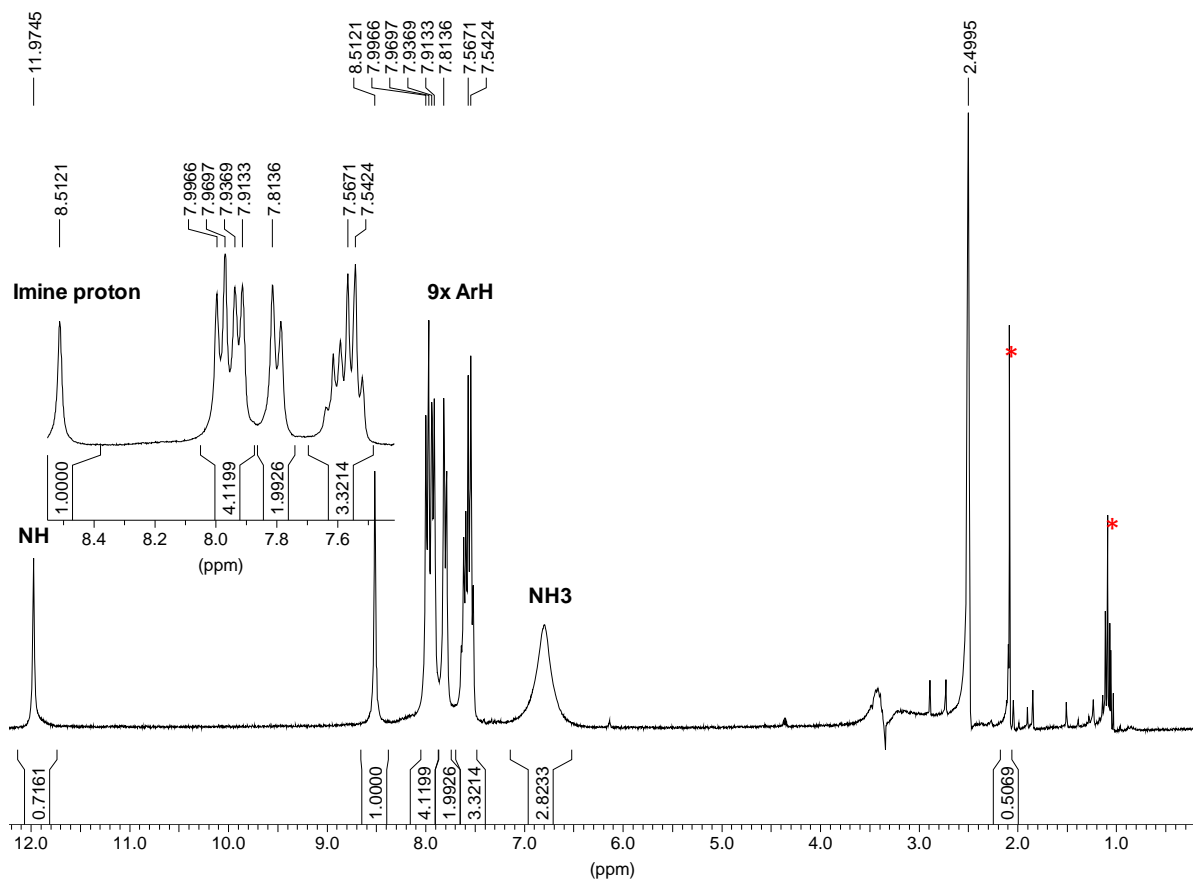
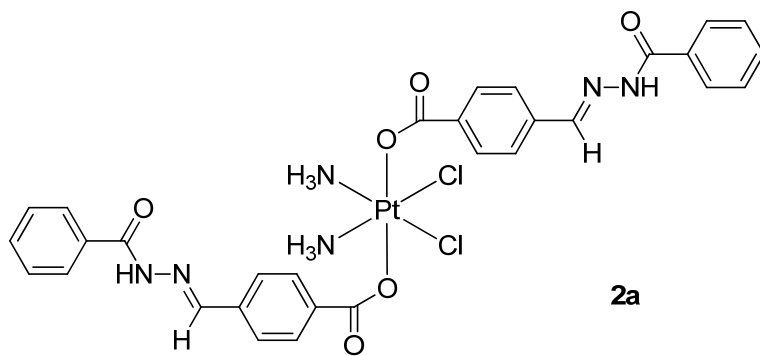


Figure S4. ^1H NMR spectra of platinum(IV)-benzhydrazone conjugate (**2a**) in DMSO-d_6 (with water suppression).

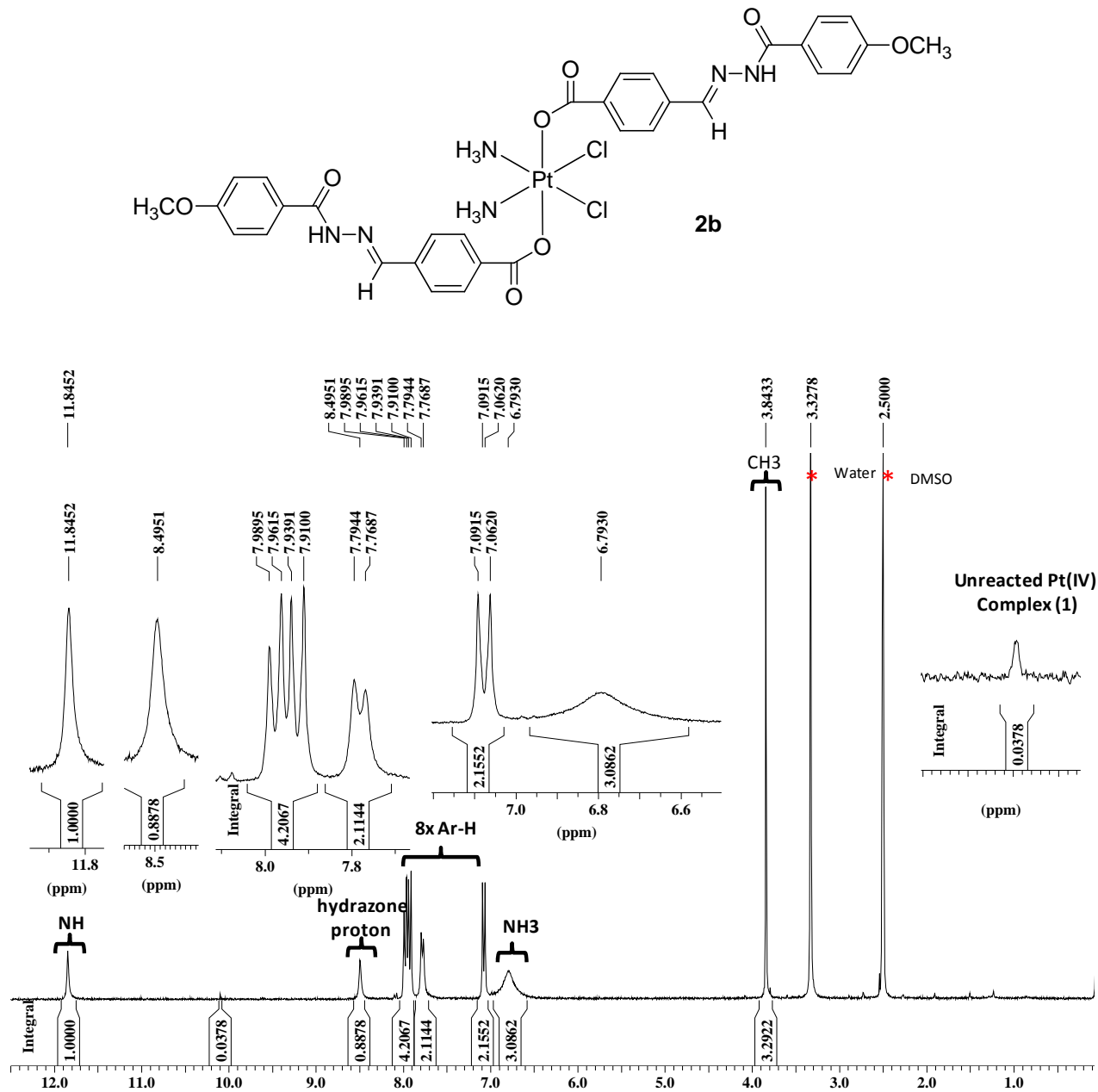
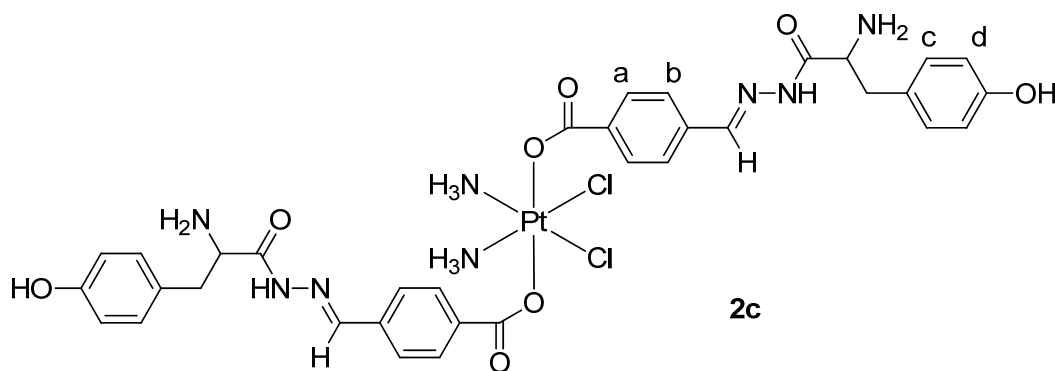
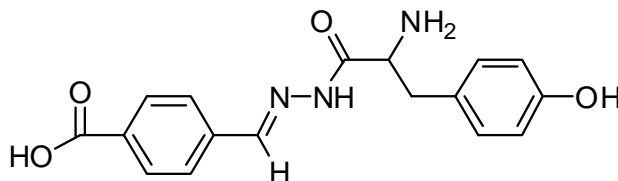


Figure S5. ^1H NMR spectra of platinum(IV)-methoxybenzhydrazone conjugate (**2b**) in DMSO- d_6 .

^1H NMR spectra of Pt-tyrosine hydrazone 2c. The asymmetry of the aromatic protons observed in the ^1H NMR spectra of **2c** was initially puzzling as the protons H_a/H_a^1 , H_b/H_b^1 and H_d/H_d^1 exhibited greater magnetic inequivalence than was observed with the other Pt(IV)-imine conjugates where the same protons (though magnetically inequivalent) had closely overlapping chemical shifts. Consequently, in order to rule out the possibility of asymmetry of the axial ligands (eg. one side having *E* stereoisomerism with the other side being *Z*), we synthesized the purely organic hydrazone conjugate between 4-carboxylbenzaldehyde and tyrosine hydrazone for comparison. As shown in Figure S6, the organic hydrazone displayed the same asymmetry of the aromatic protons. We postulated that this asymmetry arose due to slow rotation of the $\text{N}=\text{CH}-\text{Ph}$ double bond in the NMR timescale, resulting in more distinctive magnetic inequivalence of H_b vs H_b^1 .



Synthesis of hydrazone conjugate between 4-carboxylbenzaldehyde and l-tyrosine hydrazone as NMR reference. 4-carboxylbenzaldehyde (21.5 mg, 0.143 mmol) was added to a solution of l-tyrosine hydrazone (140 mg, 0.716 mmol) in 50% DMF/ H_2O (3 mL). The reaction mixture was lyophilized after 24 h and washed with H_2O to yield a white precipitate. See Figure S6 for ^1H NMR spectra; Purity (HPLC): 92% at 254 nm.



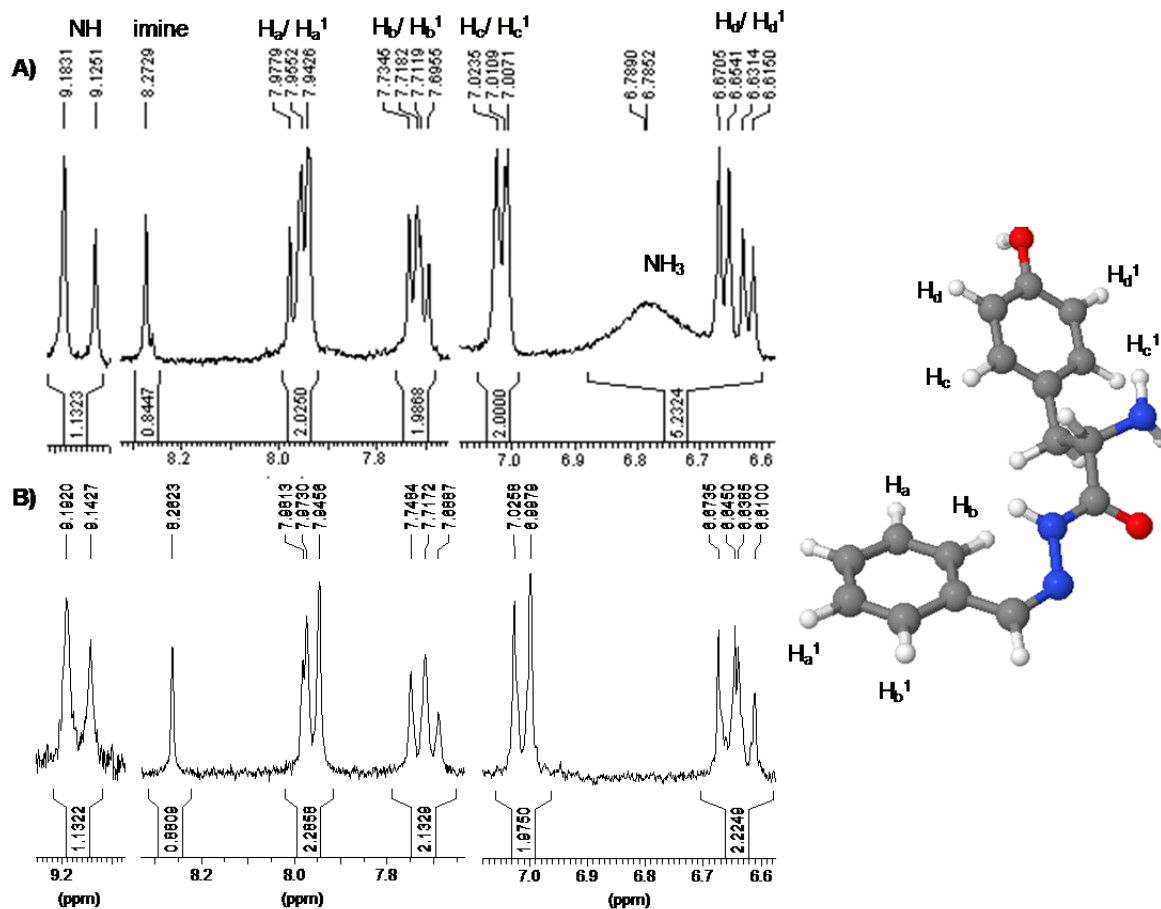


Figure S6. Similarities between 1H NMR spectrum of (A) Pt-tyrosine hydrazide (**2c**) and (B) the purely organic hydrazone ligation between 4-carboxylbenzaldehyde and tyrosine hydrazide. The 3D visual illustration is generated by CORINA.(I)

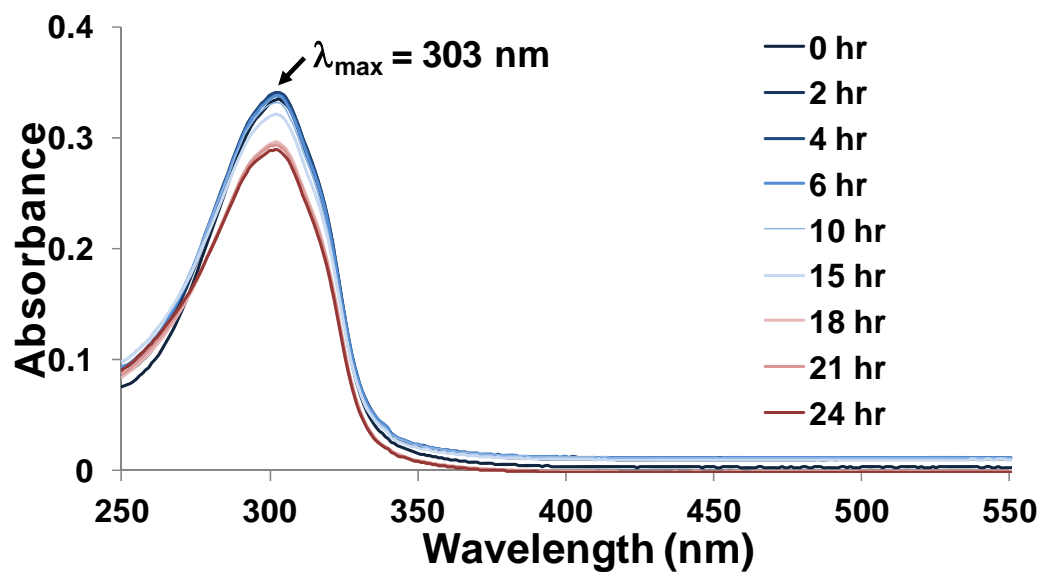
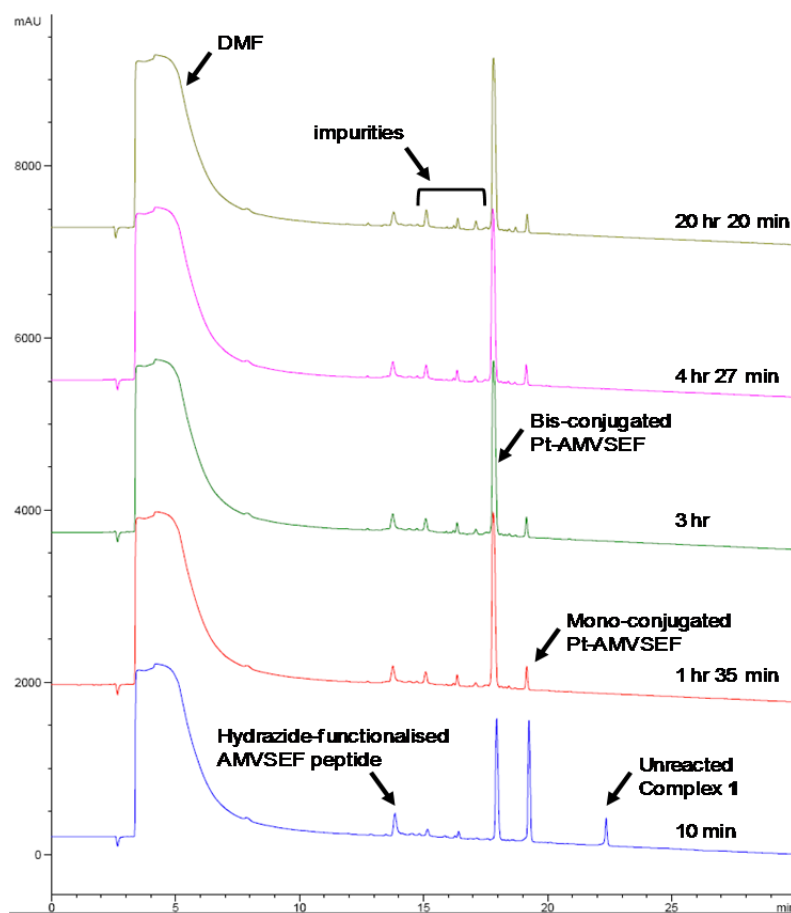


Figure S7. Only slight hydrolysis of Pt-Girard's reagent T 2e was observed at pH 7.4 and 37 °C over 24 h; the λ_{max} of the spectra was at 303 nm, attributable to the hydrazone bond.

A)



B)

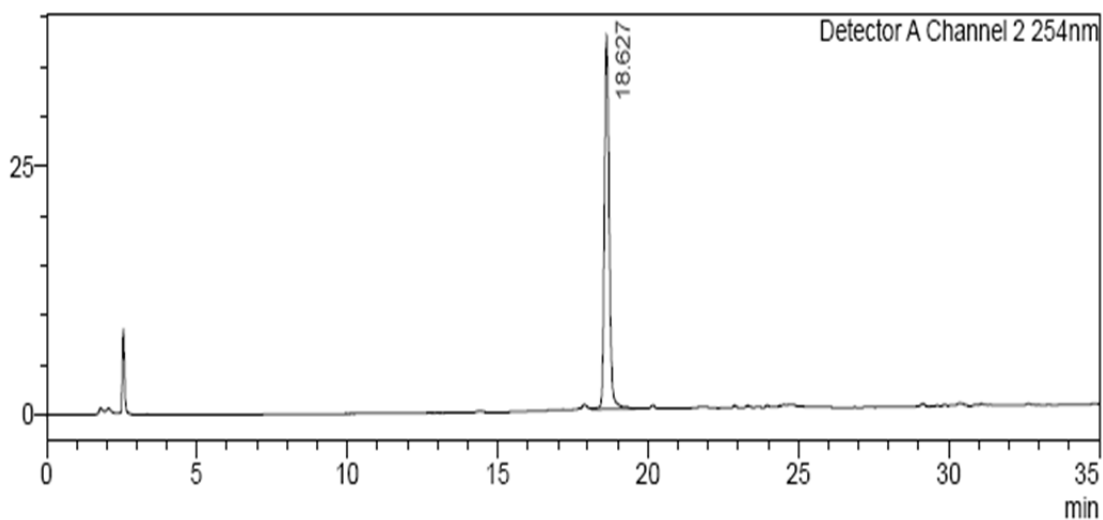


Figure S8. (A) RP-HPLC reaction monitoring of formation of Pt-AMVSEF peptide **3** at 214 nm. Elution conditions: 5 – 15% over 10 min followed by 15 – 80% from 10 to 30 min aq. NH_4OAc buffer (10 mM, pH 5.5) (solvent A) and MeCN (solvent B) at 1.0 mL/min. (B) **3** after purification by RP-HPLC.

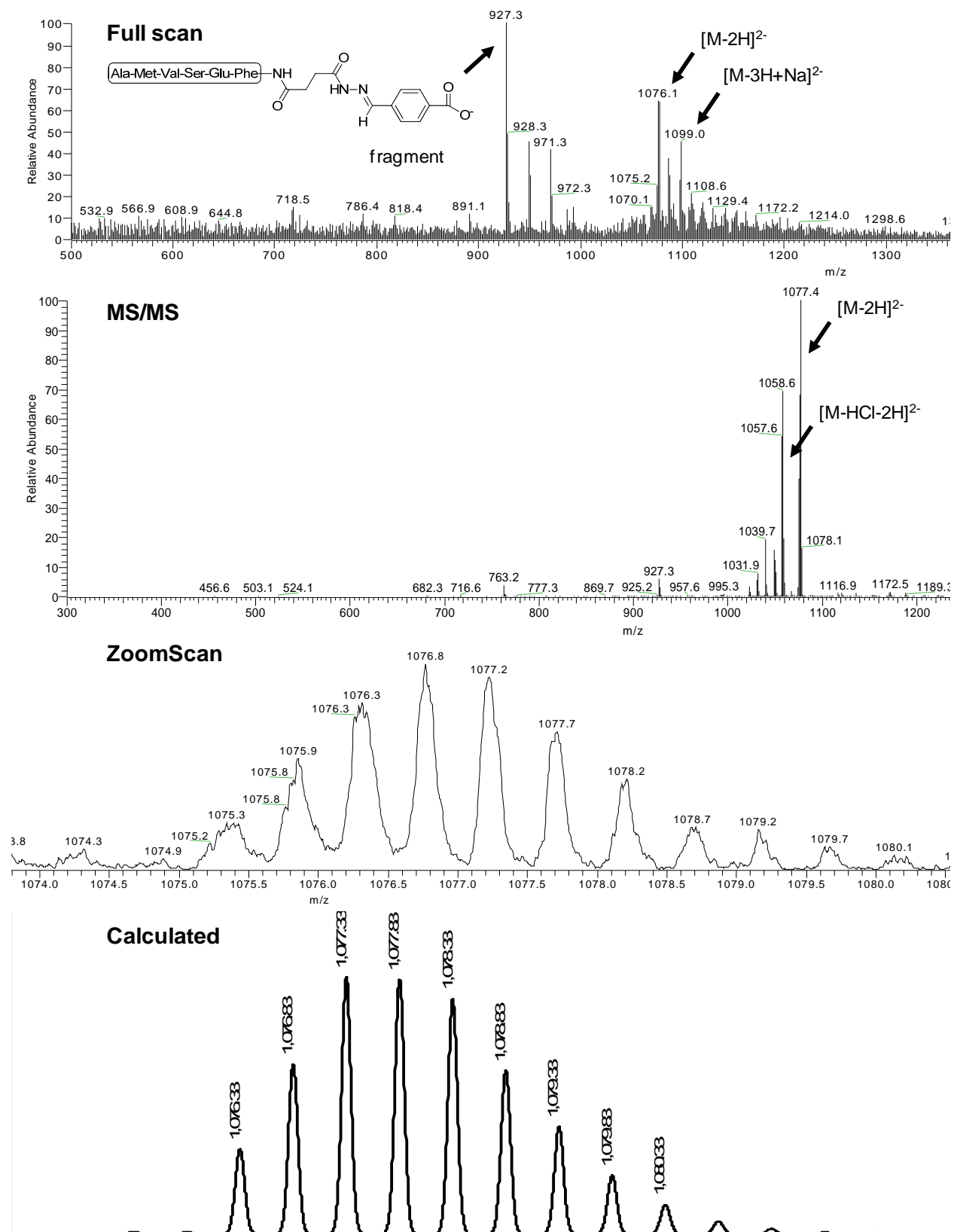


Figure S9. ESI-MS of Pt-AMVSEF peptide 3 in negative mode showing the molecular ion peak.

Catalysis at physiological pH by p-anisidine. The reaction between Pt-benzaldehyde **1** (A) and benzhydrazide to form the mono-ligated Pt-benzhydrazide (B) and bis-ligated Pt-benzhydrazide **2a** (C) product follows pseudo 1st order reaction kinetics in the presence of excess hydrazide and may be described by the following chemical equations.

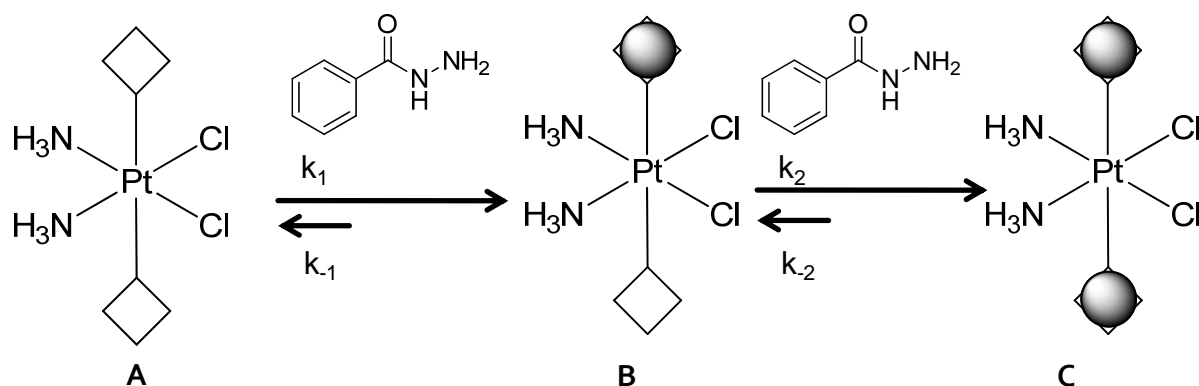


Figure S10. Illustration of imine ligation between Pt-benzaldehyde **1** (A) and benzhydrazide to yield the mono-ligated product (B) and the bis-ligated product **2a** (C).

The consumption of **1** and formation of the bis-conjugated product **2a** at hourly intervals was quantified by integration at 254 and 280 nm. In order to obtain a smooth plot of [**1**] and [**2a**] as a function of time, the experimental data was curve-fitted to model the chemical equilibria as shown in Figure S10 using the chemical reactions module of Berkeley Madonna, a commercial graphical differential equation solver.

In order to account for differences in molar absorptivity, the fraction of Pt-benzaldehyde (A) at any one point in time (t) was calculated as the current amount of A over the initial amount of A as quantified by HPLC integration. Similarly, the fraction of bis-ligated product (C) at any one point in time was calculated as the current amount of C over the maximum amount of C produced at the end of the reaction. Since it was difficult to extrapolate the maximum amount of mono-ligated product (B) from the experimental data, the fraction of B at any one point in time was calculated by subtracting from the fraction of A and C. This is summarized as the follows:

Fraction of A = Average of $\frac{\text{Absorbance of A at } t}{\text{Initial Absorbance of A at } t=0}$ at 254 and 280 nm

Fraction of C = Average of $\frac{\text{Absorbance of C at } t}{\text{Absorbance of C at } t = \infty}$ at 254 and 280 nm

Fraction of B = 1 - (Fraction of A + Fraction of C)

Table S1. Representative summary of experimental data for curve fitting. Data shown is for 100 mM p-anisidine catalysed reaction with 0.263 mM Pt-benzaldehyde and 8.71 mM benzhydrazide.

Hours	Fraction at 254nm /mAU			Fraction at 280nm /mAU			Average Fraction of 254 and 280 nm		
	1	Mono	Bis	1	Mono	Bis	1	Mono	Bis
0.00	1.00	0.00	0.00	1.00	0.00	0.00	1.00	0.00	0.00
0.17	0.97	0.03	0.00	0.94	0.06	0.00	0.95	0.05	0.00
1.00	0.86	0.14	0.00	0.80	0.20	0.00	0.83	0.17	0.00
2.08	0.76	0.24	0.00	0.77	0.23	0.00	0.76	0.24	0.00
3.17	0.69	0.31	0.00	0.67	0.33	0.00	0.68	0.32	0.00
4.25	0.71	0.29	0.00	0.72	0.28	0.00	0.72	0.28	0.00
5.33	0.62	0.38	0.00	0.63	0.36	0.01	0.63	0.37	0.00
6.42	0.56	0.44	0.01	0.52	0.47	0.01	0.54	0.45	0.01
7.50	0.50	0.48	0.01	0.46	0.52	0.01	0.48	0.50	0.01
8.50	0.45	0.53	0.02	0.41	0.57	0.02	0.43	0.55	0.02
20.50	0.18	0.71	0.11	0.18	0.71	0.11	0.18	0.71	0.11
25.50	0.16	0.67	0.17	0.19	0.64	0.17	0.18	0.66	0.17

References

- (1) Sadowski, J. G., J.; Klebe, G. (1994) Comparison of automatic three-dimensional model builders using 639 X-ray structures. *J. Chem. Inf. Model.* 34, 1000-1008.